

# Effect of tissue preservation on imaging using ultrahigh resolution optical coherence tomography

## Pei-Lin Hsiung

Massachusetts Institute of Technology  
Department of Electrical Engineering  
and Computer Science  
Research Laboratory of Electronics  
Cambridge, Massachusetts 02139

## Prashant R. Nambiar

Massachusetts Institute of Technology  
Division of Comparative Medicine  
Cambridge, Massachusetts 02139

## James G. Fujimoto

Massachusetts Institute of Technology  
Department of Electrical Engineering  
and Computer Science  
Research Laboratory of Electronics  
77 Massachusetts Avenue  
Cambridge, Massachusetts 02139  
E-mail: jgf@mit.edu

**Abstract.** Ultrahigh resolution optical coherence tomography (OCT) is an emerging imaging modality that enables noninvasive imaging of tissue with 1- to 3- $\mu\text{m}$  resolutions. Initial OCT studies have typically been performed using harvested tissue specimens (*ex vivo*). No reports have investigated postexcision tissue degradation on OCT image quality. We investigate the effects of formalin fixation and commonly used cell culture media on tissue optical scattering characteristics in OCT images at different times postexcision compared to *in vivo* conditions. OCT imaging at 800-nm wavelength with 1.5- $\mu\text{m}$  axial resolution is used to image the hamster cheek pouch *in vivo*, followed by excision and imaging during preservation in phosphate-buffered saline (PBS), Dulbecco's Modified Eagle's Media (DMEM), and 10% neutral-buffered formalin. Imaging is performed *in vivo* and at sequential time points postexcision from 15 min to 10 to 18 h. Formalin fixation results in increases in scattering intensity from the muscle layers, as well as shrinkage of the epithelium, muscle, and connective tissue of  $\sim 50\%$ . PBS preservation shows loss of optical contrast within two hours, occurring predominantly in deep muscle and connective tissue. DMEM maintains tissue structure and optical scattering characteristics close to *in vivo* conditions up to 4 to 6 h after excision and best preserved tissue optical properties when compared to *in vivo* imaging. © 2005 Society of Photo-Optical Instrumentation Engineers. [DOI: 10.1117/1.2147155]

Keywords: biomedical imaging; tissue preservation; hamster cheek pouch; optical coherence tomography; optical pathology.

Paper 05120R received May 16, 2005; revised manuscript received Aug. 24, 2005; accepted for publication Aug. 25, 2005; published online Jan. 5, 2006.

## 1 Introduction

Optical coherence tomography (OCT) is an emerging biomedical imaging modality that can generate micron-resolution, cross-sectional images of tissue microstructure *in situ* and in real time.<sup>1-3</sup> Early OCT studies initially focused on *ex vivo* imaging to establish correlations with histopathology and feasibility for future *in vivo* studies.<sup>3-15</sup> With the development of fiber optic imaging probes, *in vivo* endoscopic OCT imaging in animals was demonstrated,<sup>16</sup> and *in vivo* endoscopic imaging in humans was performed.<sup>17</sup> However, accurate registration of OCT images with histology is difficult to achieve with *in vivo* imaging. For this reason, subsequent studies investigating the effect of OCT imaging parameters on tissue structure identification in the gastrointestinal tract have been performed *ex vivo*.<sup>14</sup> Previous studies in ophthalmology have also investigated the effect of nonlinear shrinkage and sectioning stress during histology preparation on subsequent interpretation of OCT retinal images.<sup>18</sup>

It is generally believed that changes in tissue dimensions and optical characteristics occur within a few hours after tis-

sue excision, motivating investigations to be performed as soon as possible after tissue excision. OCT imaging studies of the retina show significant changes in the dimensions of intraretinal layers after excision as well as with fixation.<sup>18,19</sup> The effect of tissue ischemia on optical scattering is still not well understood. Prior OCT imaging studies in rat skin have demonstrated the use of hyperosmotic agents for reducing scattering and improving image contrast, changing OCT image penetration depths.<sup>20</sup> These studies showed negligible changes in tissue backscattering after immersion in 0.9% isotonic saline for short time periods of less than 25 min, however, longer time periods were not investigated. Near-infrared diffuse transmission and reflectance measurements have found changes in scattering and absorption coefficients after 2 h.<sup>21</sup> Fluorescence and diffuse reflectance studies have shown preservation of 70 to 90% of spectroscopic signal intensity up to 1.5 h after biopsy.<sup>22</sup> The time course of these changes postexcision has not been investigated. There has been a wide variation in imaging protocols and times postexcision. Previous studies involving *ex vivo* imaging of tissue specimens have reported imaging times after tissue excision ranging from 30 min<sup>13,23,24</sup> to 5 h.<sup>5-8</sup> Imaging has also been performed on formalin-fixed specimens,<sup>14</sup> frozen specimens,<sup>4,7</sup> and on un-

Address all correspondence to James Fujimoto, Dept. of Elect. Engin. & Computer Sci. and Research, Laboratory of Electronics, Massachusetts Institute of Technology, 77 Massachusetts Ave., Building 36-345, Cambridge, MA 02139. Tel: 617-253-8528. Fax: 617-253-9611. E-mail: jgf@mit.edu

fixed specimens harvested from cadavers.<sup>5,6,8,9,15</sup> Isotonic saline has typically been used for specimen irrigation and transport,<sup>7,10,12,13,23,25</sup> but buffered saline<sup>5,6,8,9</sup> and Hank's solution have also been used.<sup>13</sup> Studies comparing protocols for tissue preservation for *ex vivo* OCT imaging have not been reported in the literature.

The objectives of this study were to investigate the effect of formalin fixation on imaging using ultrahigh resolution OCT, and to test the effect of two commonly used laboratory culture media on *ex vivo* preservation of tissue optical scattering characteristics over time. Standard formalin fixation followed by paraffin embedding leads to shrinkage and processing artifacts, which complicate OCT image interpretation. Imaging at sequential time points during the fixation process allows one-to-one correlation of tissue structures with histology, enabling accurate interpretation of *in vivo* tissue architectural features. Since it is not always possible to image tissue specimens immediately after excision, the effect of postexcision imaging time on tissue structure and optical characteristics was also investigated. Imaging was performed on the same tissue specimens *in vivo* and up to a maximum time of 10 to 18 h after excision, enabling direct comparison of *in vivo* versus *ex vivo* imaging.

The hamster cheek pouch was chosen for this study because it consists of representative tissue components, is easily accessible, and is a commonly used system for the study of tumorigenesis. When dosed with carcinogen, histological features in this model have been shown to correspond closely with premalignant and malignant lesions in human oral mucosa.<sup>26</sup> The tissue constituents in the hamster cheek pouch are representative of the composition of human epithelial tissues such as oral mucosa, esophagus, and cervix. There has been recent interest in investigating tumor development in this model using noninvasive optical techniques. Fluorescence spectroscopy has been shown to detect biochemical changes associated with early tumor development in this model.<sup>27,28</sup> Multiphoton microscopy and optical coherence tomography have also recently demonstrated the ability to detect early morphological changes associated with cancer development in the hamster cheek pouch.<sup>29-31</sup>

In this study, three solutions were tested to assess their affect on tissue optical scattering characteristics. First, 10% neutral-buffered formalin was investigated to determine the effect of the fixation process on imaging using OCT. 10% neutral-buffered formalin, containing 4% formaldehyde, is the most common fixative used for routine paraffin-embedded sections. Formaldehyde acts by forming cross-linkages between tissue proteins, fixing cellular constituents in their *in vivo* positions and thus preventing autolytic processes.<sup>32</sup> Although formalin penetrates tissue well, the rate of tissue penetration is relatively slow.<sup>33</sup> The second solution tested was isotonic phosphate-buffered saline (PBS). PBS is a common solution used in many laboratory procedures, often serving as a medium for irrigating, transporting, and diluting fluid. Isotonic PBS maintains intra- and extracellular osmotic balance, and a buffering system keeps the medium within the physiological pH range. The third solution tested was Dulbecco's Modified Eagle's Media (DMEM), a commonly used synthetic cell culture media. DMEM includes higher concentrations of amino acids and vitamins than basal salt solutions as well as additional supplementary components, so that the me-

dium more closely approximates the protein composition of mammalian cells. Autolysis begins immediately after tissue harvest. Tissue culture media was therefore expected to slow autolytic processes, thereby slowing changes that may influence tissue contrast. Sera, which contains additional supplements and growth factors, is typically added to media used for cell culture, but it was not added to DMEM in this study because the goal was to investigate the performance of individual solutions on preservation of *in vivo* optical scattering characteristics to minimize complexity associated with tissue handling protocols.

## 2 Materials and Methods

### 2.1 OCT System Parameters

Ultrahigh resolution OCT imaging was performed using a broadband Ti:Al<sub>2</sub>O<sub>3</sub> laser-based OCT system operating at a center wavelength of 800 nm, similar to that previously described.<sup>34</sup> Imaging was performed with a measured axial resolution of 2  $\mu\text{m}$  in free space, corresponding to  $\sim 1.5 \mu\text{m}$  in tissue. To achieve high transverse resolution, an imaging probe consisting of two specially designed achromatic doublets with 10-mm focal length was used, yielding a transverse resolution of  $\sim 5 \mu\text{m}$  in air. The corresponding confocal parameter was  $\sim 140 \mu\text{m}$ . The system sensitivity was measured to be 103 dB with 3 mW of optical power on the sample. The imaging probe was mounted on two precision, computer-controlled micrometer stages to perform OCT imaging scans in two lateral dimensions. All images acquired were 1  $\times$  1 mm in dimension and consisted of 1000 axial  $\times$  1000 transverse pixels. This enabled an imaging sample density of 1 pixel/ $\mu\text{m}$  in both axial and transverse dimensions.

#### 2.1.1 Specimen selection and handling

All animal procedures were approved by the Committee on Animal Care (CAC) at the Massachusetts Institute of Technology. The Golden Syrian hamster (*Mesocricetus auratus*) cheek pouch model was chosen for this study because it consists of keratinized squamous epithelium, collagen, skeletal muscle, blood vessels, adipose tissue, and other representative tissue constituents.<sup>35</sup> Imaging in an animal model allows *in vivo* and *ex vivo* imaging to be performed on the same tissue specimen, enabling direct investigation of *ex vivo* handling protocol on image characteristics. In addition, the hamster cheek pouch carcinogenesis sequence closely resembles the events involved in the development of premalignant and malignant human oral cancers,<sup>26</sup> and thus is a relevant model for investigations of cancer progression using optical techniques. Hamsters were anesthetized using intraperitoneal pentobarbital sodium 50 mg/kg with diazepam 10 mg/kg, and kept warm using an isothermal heating pad during the *in vivo* portion of the imaging procedures.

Prior to imaging, the anesthetized hamster cheek pouch was everted using a specially designed and fabricated clamp, which was fastened rigidly to the optical table surface. Figure 1 shows a photograph of the *in vivo* and *ex vivo* imaging setup. The clamping device consisted of a top aluminum piece with a window that enabled imaging and irrigation of the tissue surface, and a bottom plastic piece that enabled the periphery of the cheek pouch specimen to be pinned postmortem. *In vivo* imaging was initially performed. The animal was

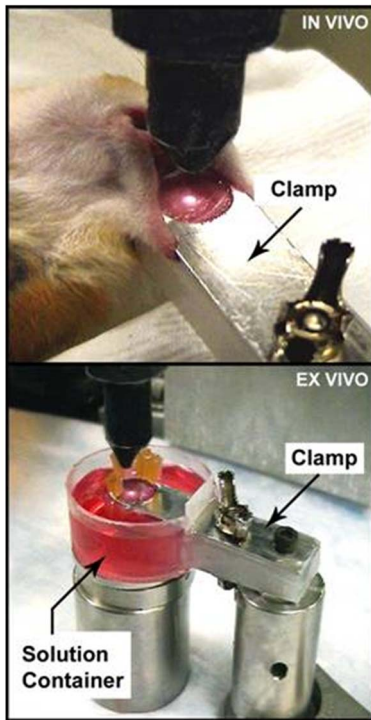


**Fig. 1** Photograph of the *in vivo* and *ex vivo* imaging experimental setup. The custom-built clamping device consisted of a top aluminum piece with a window that enabled *in vivo* imaging, and a bottom plastic piece that allowed the periphery of the cheek pouch specimen to be pinned postmortem for accurate registration during the imaging time course. A custom-designed and fabricated container around the specimen enabled complete immersion of the excised specimen in preservation solution.

subsequently euthanized and the zero time point was recorded at the time of cessation of respiration. The periphery of the cheek pouch was then pinned to the bottom piece of the clamp, enabling the cheek pouch to be excised from the animal with minimal disturbance to the *in vivo* imaging plane. Specimens of approximately  $1 \times 1$  cm size were used in this study to minimize the effect of changes in optical scattering induced by loss of local supporting tissue structure. A custom-designed and fabricated containment well was subsequently fixed around the clamp, and the specimen was immersed in 10% neutral-buffered formalin (Fisher Scientific Company, Agawam, Massachusetts), isotonic phosphate-buffered saline (OmniPur, EMD Chemicals Incorporated, Gibbstown, New Jersey), or Dulbecco's Modified Eagle's Media (Gibco/Invitrogen, Carlsbad, California). All preservation solutions were refreshed every 15 to 20 min to maintain solution tonicity. Imaging was performed at room temperature ( $21$  to  $23^\circ\text{C}$ ) to approximate the conditions present in most laboratory settings. Imaging using PBS solution was additionally performed at body temperature ( $37^\circ\text{C}$  using an isothermal heating pad) and using an ice bath (solution temperature  $8^\circ\text{C}$ ) to investigate the temperature dependence of tissue preservation over time.

## 2.2 Imaging Protocol

Separate animals were used for each solution and temperature investigated in this study to enable registered imaging *in vivo*

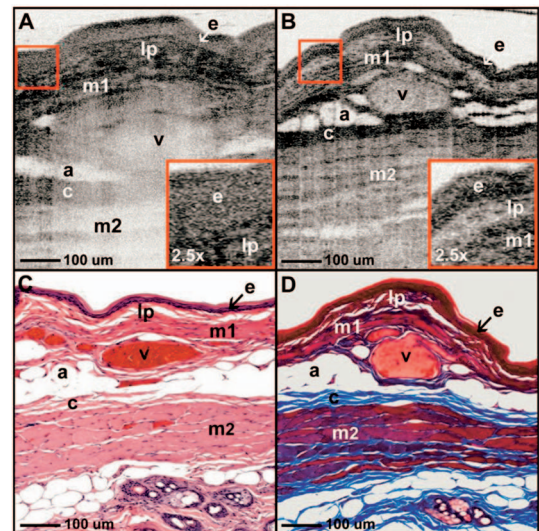


**Fig. 2** Magnified view of the cheek pouch (a) *in vivo* and (b) after fixation in formalin for 18 h with (c) hematoxylin and eosin and (d) Masson's trichrome histology. One-to-one correlation clearly identified structures corresponding to the epithelium (e), lamina propria (lp), superficial muscle layer (m1), blood vessel (v), adipocytes (a), collagen-rich connective tissue (c), and deep muscle layer (m2). Leukocytes appear in the OCT image as focal spots of increased scattering. (Wavelength 800 nm, resolution  $1.5\text{-}\mu\text{m}$  axial  $\times 5\text{-}\mu\text{m}$  transverse.)

and *ex vivo* over the entire time course. Imaging on an additional animal was performed for DMEM solution preservation to verify consistency of the observed results. For each solution, imaging was performed *in vivo*, at 15 min, 30 min, and 1, 1.5, 2, 2.5, 3, 3.5, 4, 5, 6, 7, 8, and 10 h. Imaging in formalin solution was additionally performed at 12, 14, 16, and 18 h to ensure complete fixation. For each imaging time point, 11 OCT images were taken. The focus position was set to be 200 to 250  $\mu\text{m}$  below the surface of the tissue to yield an optimum depth of field for the images. The first ten images were each sequentially offset in the sagittal direction by 100  $\mu\text{m}$ , enabling imaging over a tissue volume of  $1 \times 1 \times 1$  mm in dimension. This allowed representative images of architectural morphology of the hamster cheek pouch to be acquired and facilitated subsequent registration with histology. The final image was taken in the same location as the first image to verify the accuracy of the registration protocol and to determine if tissue optical scattering properties had changed over the course of the imaging procedure itself. Each set of 11 images was acquired in approximately 10 min. After completion of the imaging time course, the OCT imaging plane was marked with two microinjections of ink, placed in 10% neutral-buffered formalin, routinely processed, and paraffin embedded. Multiple  $5\text{-}\mu\text{m}$ -thick tissue sections were obtained from the OCT imaging planes and stained. Standard hematoxylin-eosin as well as Masson's trichrome stains were used to visualize the imaged tissues for light microscopy. OCT images and corresponding histology sections were compared. Minor discrepancies between histology and OCT images can be attributed to tissue fixation, processing, and sectioning artifacts.

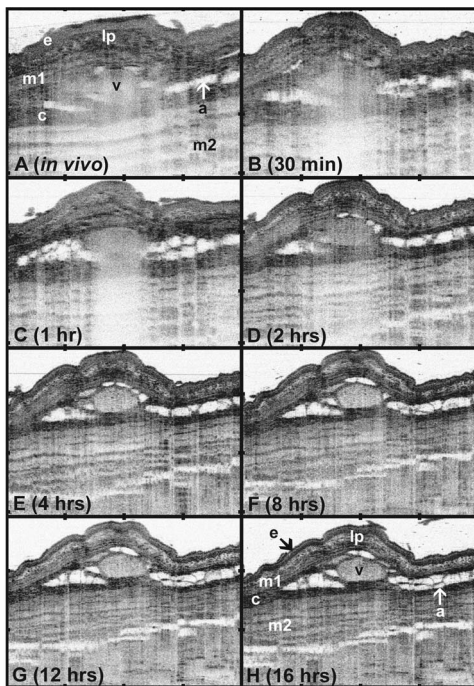


**Fig. 3** Sequence of representative OCT images acquired *in vivo* and over 16 h in 10% neutral-buffered formalin: (a) *in vivo*; (b) 30 min; (c) 1 h; (d) 2 h; (e) 4 h; (f) 8 h; (g) 12 h; (h) 16 h. Shrinkage was visible in all tissue layers. e, epithelium; lp, lamina propria; m1, m2, muscle layers; c, connective tissue; a, adipose tissue; and v, blood vessel. Tick marks represent 250  $\mu\text{m}$ . (Wavelength 800 nm, resolution 1.5- $\mu\text{m}$  axial  $\times$  5- $\mu\text{m}$  transverse.)

### 3 Results

OCT images and histology photomicrographs at 100 $\times$  and 200 $\times$  magnification are shown scaled with the same magnification as the OCT image. All OCT images were scaled in the axial direction by 1.38 $\times$  to account for the approximate index of refraction of tissue.<sup>36</sup>

#### 3.1 10% Neutral-Buffered Formalin

A magnified view of the cheek pouch *in vivo* and at 18 h with hematoxylin and eosin, and Masson's trichrome histology is shown in Fig. 2. One-to-one correlation between OCT images and histology clearly identifies the keratinized squamous epithelium, lamina propria, skeletal muscle bundles, blood vessels, adipocytes, and collagen-rich connective tissue. *In vivo*, the epithelium appeared as uniformly scattering. Muscle bundles appeared as low scattering relative to highly scattering intervening connective tissue. Collagen layers appeared relatively high scattering. Adipose tissue appeared low scattering, with distinct borders between individual adipocytes. Intravascular leukocytes in the blood vessel were seen in the OCT image as focal spots of increased scattering.

Figure 3 illustrates a sequence of representative OCT images acquired *in vivo* and over 16 h in 10% neutral-buffered formalin. During the fixation process, changes in contrast were visible within the squamous epithelial layer itself, with an increase in scattering signal in the lower 1/3 to 1/2 of the epithelium nearer the basal boundary (Fig. 2, inset). Decrease in scattering within the lamina propria was apparent, whereas

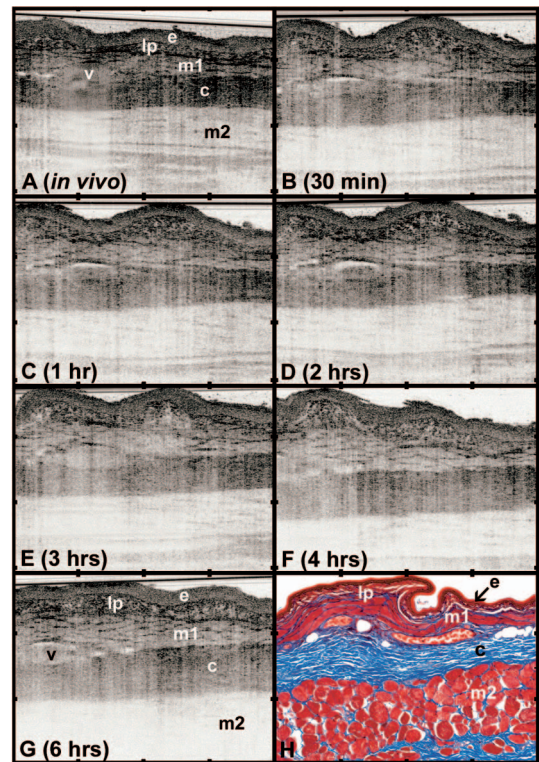


**Fig. 4** Sequence of representative OCT images acquired *in vivo* and over 6 h in isotonic phosphate-buffered saline solution at room temperature: (a) *in vivo*; (b) 30 min; (c) 1 h; (d) 2 h; (e) 3 h; (f) 4 h; (g) 6 h; (h) Masson's trichrome. Loss of scattering signal was significant within 2 h and appeared to decrease monotonically after tissue excision. Swelling in the muscle (m1 and m2) and thick connective tissue layer (c) was visible. e, epithelium; lp, lamina propria; and v, blood vessel. Tick marks represent 250  $\mu\text{m}$ . (Wavelength 800 nm, resolution 1.5- $\mu\text{m}$  axial  $\times$  5- $\mu\text{m}$  transverse.)

scattering within muscle bundles appeared to increase. Overall contrast between tissue architectural features appeared to increase during fixation over 18 h and corresponded in time with significantly noticeable tissue shrinkage. Shrinkage was visible in the deeper muscle bundle and connective tissue layers by 1 h after immersion in formalin, and increase in scattering was significantly noticeable by 2 h. The squamous epithelial layer, loose connective tissue, and muscle layers exhibited approximately 50% overall shrinkage. Little or no shrinkage was observed in adipose tissue; however, boundaries between adipocytes sharpened over the 18 h time course. Shrinkage and distortion of the surrounding connective tissue is most likely responsible for visible architectural changes in the adipose tissue layers. A large blood vessel visible at the center of the image also exhibited shadowing *in vivo* and over the first 2 h, which disappeared completely by 4 h.

#### 3.2 Isotonic Phosphate-Buffered Saline

Figure 4 illustrates OCT images acquired *in vivo* and over 6 h after excision and immersion in isotonic phosphate-buffered saline at room temperature. The appearance of tissue architectural features *in vivo* was consistent with the *in vivo* appearance of the formalin time course specimen discussed previ-

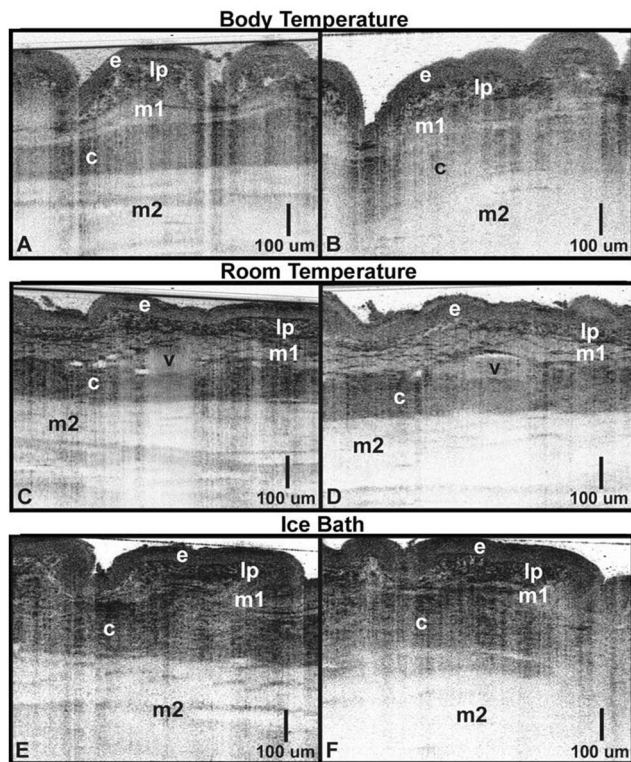


**Fig. 5** Images acquired [(a), (c), and (e)] *in vivo* and [(b), (d), and (f)] at 6 h postexcision obtained after immersion in PBS at body temperature (top), room temperature (middle), and under hypothermic conditions (bottom). Tissue maintained at body temperature in PBS saline seemed to preserve higher scattering signal intensity in the deeper tissue layers relative to PBS at room temperature and using an ice bath, although differences were not significant. e, epithelium; lp, lamina propria; m1, m2, muscle layers; c, connective tissue; and v, blood vessel. (Wavelength 800 nm, resolution 1.5- $\mu\text{m}$  axial  $\times$  5- $\mu\text{m}$  transverse.)

ously. However, postexcision, the optical scattering intensity appeared to decrease monotonically after immersion in PBS. Decrease in overall signal intensity was visible in the image within 30 min after tissue excision and was significant by 2 h. Loss of the optical scattering signal appeared first in the deeper muscle and connective tissue layer (m2) and was consistently noticeable within 3 to 4 h. Swelling in the superficial muscle (m1) and thick connective tissue layer (c) was visible. Settling of blood vessel contents was visible in some images, as was distortion of vessel walls. Significant overall changes in the epithelial layer were not observed during immersion in isotonic PBS at room temperature over the 10-h time course, although shrinkage is visible in the histology due to formalin fixation.

Figure 5 illustrates images acquired *in vivo* and at 6-h postexcision obtained after immersion in PBS at body temperature, room temperature, and under hypothermic conditions. Each of the separate tissue specimens exhibited loss of scattering signal in the deeper muscle and connective tissue layer (m2) by 3 to 4 h, which were significantly noticeable by 6 h. Tissue maintained at body temperature in PBS saline seemed to preserve higher signal intensity in the deeper muscle layers relative to PBS at room temperature and using an ice bath,

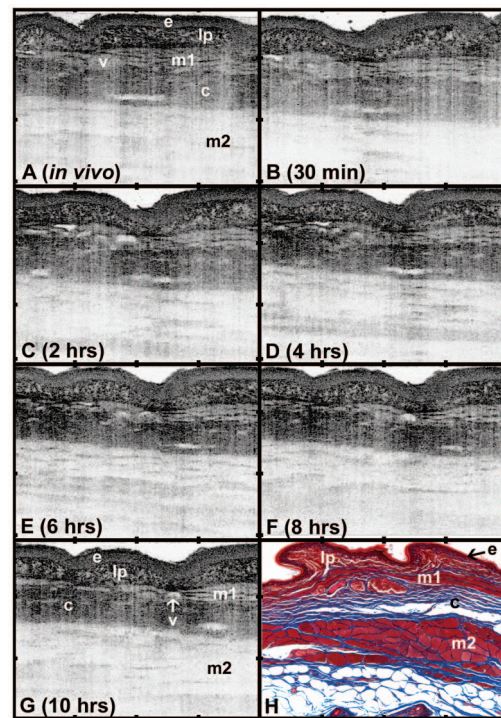


**Fig. 6** Sequence of representative OCT images acquired *in vivo* and over 10 h in DMEM solution at room temperature: (a) *in vivo*; (b) 30 min; (c) 2 h; (d) 4 h; (e) 6 h; (f) 8 h; (g) 10 h; (h) Masson's trichrome. Optical scattering characteristics were maintained close to *in vivo* conditions up to 4 to 6 h after excision and remained similar over the entire time course. Note that the time points illustrated before are different from those illustrated in Fig. 4 because of the longer time course of visible changes during immersion in DMEM. e, epithelium; lp, lamina propria; m1, m2, muscle layers; c, connective tissue; and v, blood vessel. Tick marks represent 250  $\mu\text{m}$ . (Wavelength 800 nm, resolution 1.5- $\mu\text{m}$  axial  $\times$  5- $\mu\text{m}$  transverse.)

although differences were not significant. Some swelling of the superficial muscle layer (m1) and thick connective tissue layer (c) was observed at all temperatures.

### 3.3 Dulbecco's Modified Eagle's Media

Figure 6 illustrates OCT images acquired *in vivo* and over 10 h after excision and immersion in DMEM at room temperature. Note that the time points of the images in Fig. 6 were chosen to illustrate the time course of changes occurring during immersion in DMEM and are different from the time points illustrated in Fig. 4. Visualization of tissue architectural morphology *in vivo* was also consistent with *in vivo* imaging for both formalin and PBS specimens discussed previously. Scattering signal intensity was maintained close to *in vivo* conditions during immersion in DMEM up to 4 to 6 h after excision. A slight decrease of scattering signal visible at the 6 to 8 h time point also appeared first in the deep muscle and connective tissue layer (m2), but was not significantly noticeable until 8 to 10 h after tissue excision. No significant overall swelling in any of the tissue layers was observed during immersion in DMEM at room temperature. Significant changes in the epithelial layer were not observed during immersion in DMEM at room temperature over the 10-h time course, although shrinkage is again visible in the histology

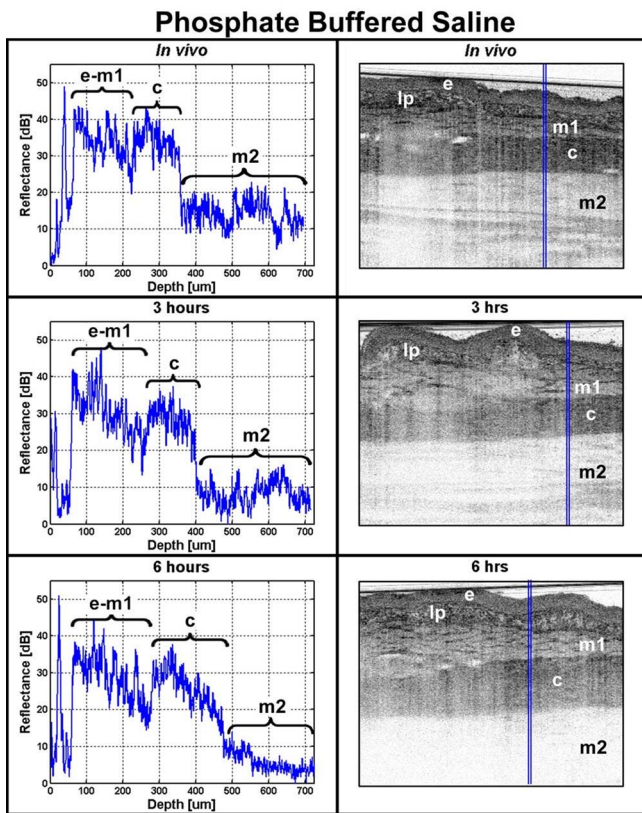


**Fig. 7** Measured reflectance profiles as a function of depth for PBS *in vivo*, at 4 h and at 10 h. Profiles were averaged over ten consecutive axial scans to reduce noise fluctuations. Scan profiles for PBS show a loss of contrast between layers over the time course and a decrease in overall signal intensity, particularly in the deep muscle and connective tissue layers. e, epithelium; lp, lamina propria; m1, m2, muscle layers; and c, connective tissue.

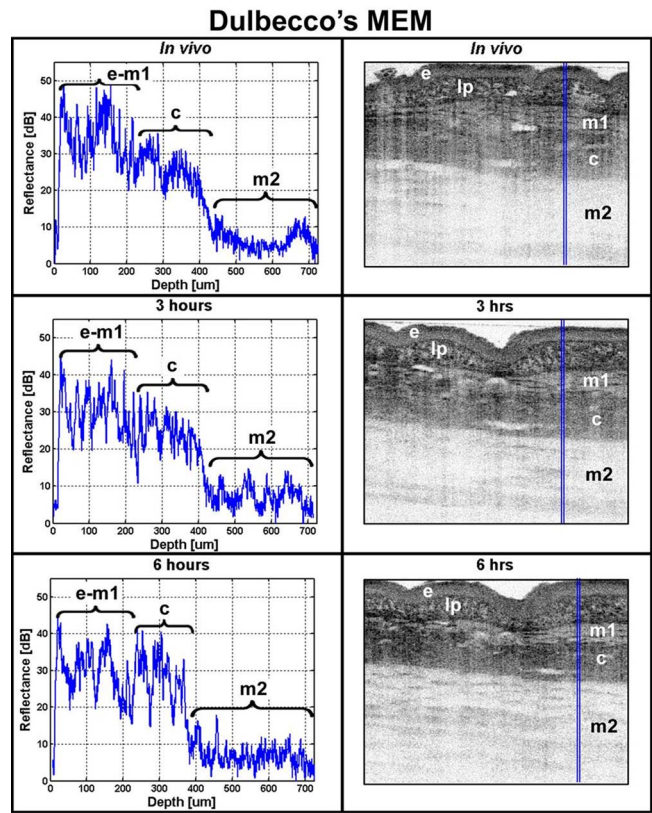


**Fig. 8** Measured reflectance profiles as a function of depth for DMEM *in vivo*, at 4 h and at 10 h. Profiles were averaged over ten consecutive axial scans to reduce noise fluctuations. Overall contrast and scattering signal intensity for DMEM was preserved similar to *in vivo* conditions. e, epithelium; lp, lamina propria; m1, m2, muscle layers; and c, connective tissue.

due to formalin fixation. Preservation in DMEM maintained the most similar image appearance and overall signal intensity compared with *in vivo* imaging.

Figures 7 and 8 show a comparison of representative axial scan profiles for DMEM and PBS *in vivo* at 4 h and 10 h. Scan profiles were averaged over ten consecutive axial scans to minimize fluctuations due to noise. Axial scan profiles for PBS show a loss of signal intensity between layers over the time course and a decrease in overall reflectivity, particularly in the deep muscle and connective tissue layers. The overall tissue scattering signal compared to *in vivo* conditions was best preserved using DMEM.

#### 4 Discussion

*Ex vivo* investigations are often a necessary step in the process of validating new technologies and devices for clinical applications. *Ex vivo* imaging has the advantage of allowing careful control of imaging parameters difficult to perform *in vivo*, enabling accurate registration of images with histology and allowing feasibility for future *in vivo* studies to be established.

Since it is not always possible in studies with human tissue to image specimens immediately after excision, the impact of postexcision imaging time and specimen handling protocol needs to be assessed to minimize deviation of tissue *ex vivo*

optical scattering properties from those observed *in vivo*. Effects of ischemia, such as cell lysis, alter tissue microstructure and, therefore, could affect optical scattering and imaging contrast. In addition, standard postexcision fixation and paraffin embedding may result in processing artifacts that can complicate image interpretation.

The objectives of this study were to investigate the effect of formalin fixation on imaging using optical coherence tomography, and to test the effectiveness of two commonly available laboratory solutions for *ex vivo* preservation of optical scattering over time. Accurate registration of images with histology is particularly difficult to achieve with *in vivo* imaging. Prior studies have relied on animal models using architectural landmarks to interpret tissue structures.<sup>19</sup> Imaging through the fixation process minimizes artifacts introduced by fixation and allows one-to-one correlation of tissue structures with histology, enabling direct interpretation of *in vivo* tissue architectural features.

In this study, the formalin-fixation process led to changes in scattering and tissue architectural distortion due to shrinkage of epithelial, muscle, and connective tissue layers. This is consistent with results reported for human colorectal resection specimens,<sup>37</sup> as well as for retinal specimens.<sup>18</sup> Formalin solution is hyperosmotic relative to tissue, therefore the shrinkage and scattering changes visible in OCT images may be due

to tissue dehydration. Recent studies investigating the effect of hyperosmotic agents have shown that local dehydration may contribute to increased scattering due to greater packing of inter- and intracellular tissue components, which contribute to scattering.<sup>20,23,38</sup> In addition, the extensive cross-linking of tissue proteins by formalin changes the tissue microstructural features and are likely to cause changes in tissue optical scattering properties. Changes in optical scattering during fixation, therefore, likely result from a combination of alterations in tissue structural properties due to the fixation process and overall tissue dehydration. Although significant distortion was evident during the fixation process, comparison of OCT images of fixed specimens with histology showed that little cumulative structural artifact was introduced during subsequent processing and sectioning.

Tissue preservation in PBS solutions resulted in gradual loss of tissue scattering intensity over time, with some appearance of swelling in the superficial muscle and thick connective tissue layer. Although significant changes in optical scattering characteristics were initially expected within 30 min, pronounced changes in PBS were not evident until 2 h after tissue excision. Loss of scattering signal was most evident in the deep muscle and connective tissue layer. In contrast, preservation in DMEM solution yielded only slight loss of overall scattering signal over the entire time course, and little tissue shrinkage or swelling. For both solutions, little overall change was visible in the keratinized squamous epithelial layer over the entire time course. These results are consistent with examination of histology specimens from PBS and DMEM solutions. Histology from PBS solutions showed evidence of mild to moderate edema of the underlying connective tissue stroma, which was not evident in histology from the DMEM solution. Therefore, it is possible that while dehydration contributes to increased scattering in the case of formalin, edema results in a decrease in packing of tissue components and a loss of scattering, particularly in the connective tissue layers, which may expand to absorb excess fluid more readily. The osmolarity of PBS (~308 mOsm) is somewhat lower than that of DMEM (~366 mOsm); therefore, hydration and swelling is more likely during immersion in PBS solution. No postmortem autolysis was observed in any of the specimens, although evidence of subtle cellular changes in the epithelium, such as mild to moderate intracellular edema and swollen nuclei with open chromatin, was present, which could demonstrate the effect of the preservation solutions.

Tissue preserved at body temperature in PBS saline seemed to maintain slightly higher signal intensity in the deep muscle and connective tissue layers relative to PBS at room temperature and using an ice bath, although differences were not significant. *In vivo* tissue scattering characteristics were expected to be best preserved using an ice bath, because cryopreservation is known to slow metabolic processes, which result in accumulation of metabolic wastes and hasten tissue autolysis. Lack of a significant effect of temperature on optical scattering over time suggests that inherent cellular metabolic processes did not significantly contribute to visible architectural changes within the investigated 10-h time course. Tissue edema is therefore likely the dominant effect resulting in decreased optical scattering over the first 10 h after excision. This is consistent with histology from the specimens,

which showed no significant differences between tissue specimens maintained at different temperatures. It is also possible that changes in tissue scattering characteristics were not dramatic postexcision because the hamster cheek pouch is relatively stable when compared to other types of tissues and less sensitive to autolytic processes. Tissues with more fragile morphology, such as gastric cardia or colonic mucosa, may experience faster postmortem tissue autolysis and be more sensitive to *ex vivo* handling protocol.

The relative scattering intensity of tissue layers was consistent for all solutions both *in vivo* and *ex vivo* over the imaging time course for both PBS and DMEM solutions. The squamous epithelium was observed to be uniform and relatively low scattering when compared to the underlying lamina propria, and collagen and loose connective tissues were more highly scattering than the muscle bundles. These observations are similar to results reported *in vivo* and *ex vivo* for human esophagus, which consists of a uniform and lower scattering unkeratinized squamous epithelium, a lower scattering muscularis layer, and higher scattering collagen-rich lamina propria and submucosa.<sup>14,25,39</sup> Discrepancy between *in vivo* and *ex vivo* layer thicknesses have been observed, which may be attributed to shrinkage due to fixation as well as specimen stretching and pinning artifacts.<sup>14</sup>

In this study, the focus zone of the image was held consistently 200 to 250  $\mu\text{m}$  below the surface of the tissue. This enabled comparison between images, but depth of field limitations may lead to different appearances of layers with the same tissue constituents. For example, the connective tissue of the lamina propria in the hamster cheek pouch appears with noticeable fine structure, while the thick connective tissue layer deeper in the tissue appears as a more uniformly scattering band. This may also be partially due to different tissue morphology and composition. It is likely that focus tracking methods<sup>34,40</sup> would yield a more consistent appearance of tissue layers in OCT images.

## 5 Conclusion

Ultrahigh resolution OCT consistently identified the normal keratinized squamous epithelial layer, lamina propria, collagen, muscle bundles, blood vessels, and adipose tissue *in vivo* and *ex vivo*. Formalin fixation can result in significant shrinkage of all tissue layers, resulting in tissue architectural distortion. Imaging through the fixation process allows one-to-one correlation of hamster cheek pouch structures with histology, enabling accurate interpretation of *in vivo* tissue architectural features. Changes in optical scattering are significant within the first 2-h postexcision after preservation with isotonic PBS. DMEM best preserves *in vivo* tissue scattering characteristics over the 10-h imaging time course. While neoplastic lesions are not evaluated in this study, it is expected that similar benefits of imaging using DMEM or other tissue culture media would also apply. Preservation at body temperature using PBS seems slightly better than either room temperature or cold preservation, although differences are not significant. These results suggest that a tissue culture environment is preferable for preparation of recently excised tissue specimens for optical imaging. These results can also be used as a baseline to aid interpretation of tumor progression studies in the hamster cheek pouch model using optical methods.

## Acknowledgments

The authors gratefully acknowledge financial support under National Institutes of Health RO1-CA75289-06, National Science Foundation ECS-01-19452 and BES-0119494, Air Force Office of Scientific Research Medical Free Electron Laser Program F49620-01-1-0186, the Poduska Family Foundation Fund for Innovative Research in Cancer, and through the philanthropy of Gerhard Andlinger. We thank Yu Chen for assistance with animal handling and helpful discussions, and Kathleen Cormier for help with histology registration and processing. We gratefully acknowledge Costas Pitris and Tony Ko for their contributions to the early phases of this study.

## References

- D. Huang, E. A. Swanson, C. P. Lin, J. S. Schuman, W. G. Stinson, W. Chang, M. R. Hee, T. Flotte, K. Gregory, C. A. Puliafito, and J. G. Fujimoto, "Optical coherence tomography," *Science* **254**(5035), 1178–1181 (1991).
- J. G. Fujimoto, M. E. Brezinski, G. J. Tearney, S. A. Boppart, B. Bouma, M. R. Hee, J. F. Southern, and E. A. Swanson, "Optical biopsy and imaging using optical coherence tomography," *Nat. Med.* **1**(9), 970–972 (1995).
- M. E. Brezinski, G. J. Tearney, B. E. Bouma, J. A. Izatt, M. R. Hee, E. A. Swanson, J. F. Southern, and J. G. Fujimoto, "Optical coherence tomography for optical biopsy. Properties and demonstration of vascular pathology," *Circulation* **93**(6), 1206–1213 (1996).
- J. A. Izatt, M. D. Kulkarni, W. Hsing-Wen, K. Kobayashi, and M. V. Sivak, Jr., "Optical coherence tomography and microscopy in gastrointestinal tissues," *IEEE J. Sel. Top. Quantum Electron.* **2**(4), 1017–1028 (1996).
- G. J. Tearney, M. E. Brezinski, J. F. Southern, B. E. Bouma, S. A. Boppart, and J. G. Fujimoto, "Optical biopsy in human gastrointestinal tissue using optical coherence tomography," *Am. J. Gastroenterol.* **92**(10), 1800–1804 (1997).
- G. J. Tearney, M. E. Brezinski, J. F. Southern, B. E. Bouma, S. A. Boppart, and J. G. Fujimoto, "Optical biopsy in human urologic tissue using optical coherence tomography," *J. Urol. (Baltimore)* **157**(5), 1915–1919 (1997).
- K. Kobayashi, J. A. Izatt, M. D. Kulkarni, J. Willis, and M. V. Sivak, Jr., "High-resolution cross-sectional imaging of the gastrointestinal tract using optical coherence tomography: preliminary results," *Gastrointest Endosc* **47**(6), 515–523 (1998).
- G. J. Tearney, M. E. Brezinski, J. F. Southern, B. E. Bouma, S. A. Boppart, and J. G. Fujimoto, "Optical biopsy in human pancreaticobiliary tissue using optical coherence tomography," *Dig. Dis. Sci.* **43**(6), 1193–1199 (1998).
- C. Pitris, M. E. Brezinski, B. E. Bouma, G. J. Tearney, J. F. Southern, and J. G. Fujimoto, "High resolution imaging of the upper respiratory tract with optical coherence tomography—A feasibility study," *Am. J. Respir. Crit. Care Med.* **157**(5), 1640–1644 (1998).
- C. Pitris, A. Goodman, S. A. Boppart, J. J. Libus, J. G. Fujimoto, and M. E. Brezinski, "High-resolution imaging of gynecologic neoplasms using optical coherence tomography," *Obstet. Gynecol. (N.Y., N.Y., U.S.)* **93**(1), 135–139 (1999).
- C. A. Jessor, S. A. Boppart, C. Pitris, D. L. Stamper, G. P. Nielsen, M. E. Brezinski, and J. G. Fujimoto, "High resolution imaging of transitional cell carcinoma with optical coherence tomography: feasibility for the evaluation of bladder pathology," *J. Radiol.* **72**(864), 1170–1176 (1999).
- C. Pitris, C. Jessor, S. A. Boppart, D. Stamper, M. E. Brezinski, and J. G. Fujimoto, "Feasibility of optical coherence tomography for high-resolution imaging of human gastrointestinal tract malignancies," *J. Gastroenterol.* **35**(2), 87–92 (2000).
- A. V. D'Amico, M. Weinstein, X. Li, J. P. Richie, and J. Fujimoto, "Optical coherence tomography as a method for identifying benign and malignant microscopic structures in the prostate gland," *Urology* **55**(5), 783–787 (2000).
- I. Cilesiz, P. Fockens, R. Kerindongo, D. Faber, G. Tytgat, F. Ten Kate, and T. Van Leeuwen, "Comparative optical coherence tomography imaging of human esophagus: how accurate is localization of the muscularis mucosae?" *Gastrointest Endosc* **56**(6), 852–857 (2002).
- L. Pantanowitz, P. L. Hsiung, T. H. Ko, K. Schneider, P. R. Herz, J. G. Fujimoto, S. Raza, and J. L. Connolly, "High-resolution imaging of the thyroid gland using optical coherence tomography," *Head Neck* **26**(5), 425–434 (2004).
- G. J. Tearney, M. E. Brezinski, B. E. Bouma, S. A. Boppart, C. Pitvis, J. F. Southern, and J. G. Fujimoto, "In vivo endoscopic optical biopsy with optical coherence tomography," *Science* **276**(5321), 2037–2039 (1997).
- A. M. Sergeev, V. M. Gelikonov, G. V. Gelikonov, F. I. Feldchtein, R. V. Kuranov, N. D. Gladkova, N. M. Shakhova, L. B. Snopova, A. V. Shakov, I. A. Kuznetsova, A. N. Denisenko, V. V. Pochinko, Y. P. Chumakov, and O. S. Streltsova, "In vivo endoscopic OCT imaging of precancer and cancer states of human mucosa," *Opt. Express* **1**(13), 432 (1997).
- E. M. Anger, A. Unterhuber, B. Hermann, H. Sattmann, C. Schubert, J. E. Morgan, A. Cowey, P. K. Ahnelt, and W. Drexler, "Ultrahigh resolution optical coherence tomography of the monkey fovea. Identification of retinal sublayers by correlation with semithin histology sections," *Exp. Eye Res.* **78**(6), 1117–1125 (2004).
- M. Gloesmann, B. Hermann, C. Schubert, H. Sattmann, P. K. Ahnelt, and W. Drexler, "Histologic correlation of pig retina radial stratification with ultrahigh-resolution optical coherence tomography," *Invest. Ophthalmol. Visual Sci.* **44**(4), 1696–1703 (2003).
- R. K. Wang, X. Xu, V. V. Tuchin, and J. B. Elder, "Concurrent enhancement of imaging depth and contrast for optical coherence tomography by hyperosmotic agents," *J. Opt. Soc. Am. B* **18**(7), 948–953 (2001).
- Y. Du, X. H. Hu, M. Cariveau, X. Ma, G. W. Kalmus, and J. Q. Lu, "Optical properties of porcine skin dermis between 900 nm and 1500 nm," *Phys. Med. Biol.* **46**(1), 167–181 (2001).
- G. M. Palmer, C. L. Marshek, K. M. Vrotsos, and N. Ramanujam, "Optimal methods for fluorescence and diffuse reflectance measurements of tissue biopsy samples," *Lasers Surg. Med.* **30**(3), 191–200 (2002).
- R. K. Wang and J. B. Elder, "Propylene glycol as a contrasting agent for optical coherence tomography to image gastrointestinal tissues," *Lasers Surg. Med.* **30**(3), 201–208 (2002).
- B. Shen, G. Zuccaro, T. L. Gramlich, N. Gladkova, B. A. Lashner, C. P. Delaney, J. T. Connor, F. H. Remzi, M. Kareta, C. L. Bevins, F. Feldchtein, S. A. Strong, M. L. Bambrick, P. Trolli, and V. W. Fazio, "Ex vivo histology-correlated optical coherence tomography in the detection of transmural inflammation in Crohn's disease," *Gastroenterol. Hepatol.* **2**(9), 754–760 (2004).
- X. D. Li, S. A. Boppart, J. Van Dam, H. Mashimo, M. Mutinga, W. Drexler, M. Klein, C. Pitris, M. L. Krinsky, M. E. Brezinski, and J. G. Fujimoto, "Optical coherence tomography: advanced technology for the endoscopic imaging of Barrett's esophagus," *Endoscopy* **32**(12), 921–930 (2000).
- D. G. MacDonald, "Comparison of epithelial dysplasia in hamster cheek pouch carcinogenesis and human oral mucosa," *J. Oral Pathol.* **10**(3), 186–191 (1981).
- L. Coghlan, U. Utzinger, R. Drezek, D. Heintzelman, A. Zuluaga, C. Brookner, R. Richards-Koryum, I. Gimenez-Conti, and M. Follen, "Optimal fluorescence excitation wavelengths for detection of squamous intra-epithelial neoplasia: results from an animal model," *Opt. Express* **7**(12) 436–446(2000).
- L. Coghlan, U. Utzinger, R. Richards-Kortum, C. Brookner, A. Zuluaga, I. Gimenez-Conti, and M. Follen, "Fluorescence spectroscopy of epithelial tissue throughout the dysplasia-carcinoma sequence in an animal model: spectroscopic changes precede morphologic changes," *Lasers Surg. Med.* **29**(1), 1–10 (2001).
- P. Wilder-Smith, K. Osann, N. Hanna, N. El Abbadi, M. Brenner, D. Messadi, and T. Krasieva, "In vivo multiphoton fluorescence imaging: a novel approach to oral malignancy," *Lasers Surg. Med.* **35**(2), 96–103 (2004).
- P. Wilder-Smith, W. G. Jung, M. Brenner, K. Osann, H. Beydoun, D. Messadi, and Z. Chen, "In vivo optical coherence tomography for the diagnosis of oral malignancy," *Lasers Surg. Med.* **35**, 269–275 (2004).
- E. S. Matheny, N. M. Hanna, W. G. Jung, Z. Chen, P. Wilder-Smith, R. Mina-Araghi, and M. Brenner, "Optical coherence tomography of malignancy in hamster cheek pouches," *J. Biomed. Opt.* **9**(5), 978–981 (2004).
- A. G. E. Pearse, *Histochemistry, Theoretical and Applied*, 4 ed.,

- Church Livingstone, New York (1991).
33. R. D. Start, C. M. Layton, S. S. Cross, and J. H. Smith, "Reassessment of the rate of fixative diffusion," *J. Clin. Pathol.* **45**(12), 1120–1121 (1992).
  34. W. Drexler, U. Morgner, F. X. Kärtner, C. Pitris, S. A. Boppart, X. D. Li, E. P. Ippen, and J. G. Fujimoto, "In vivo ultrahigh resolution optical coherence tomography," *Opt. Lett.* **24**, 1221–1223 (1999).
  35. N. G. Ghoshal and H. S. Bal, "Histomorphology of the hamster cheek pouch," *Lab Anim.* **24**, 228–233 (1990).
  36. A. Knüttel and M. Boehlau-Godau, "Spatially confined and temporally resolved refractive index and scattering evaluation in human skin performed with optical coherence tomography," *J. Biomed. Opt.* **5**(1), 83–92 (2000).
  37. N. S. Goldstein, A. Soman, and J. Sacksner, "Disparate surgical margin lengths of colorectal resection specimens between in vivo and in vitro measurements. The effects of surgical resection and formalin fixation on organ shrinkage," *Am. J. Clin. Pathol.* **111**(3), 349–351 (1999).
  38. Y. He and R. K. Wang, "Dynamic optical clearing effect of tissue impregnated with hyperosmotic agents and studied with optical coherence tomography," *J. Biomed. Opt.* **9**(1), 200–206 (2004).
  39. G. Zuccaro, N. Gladkova, J. Vargo, F. Feldchtein, E. Zagaynova, D. Conwell, G. Falk, J. Goldblum, J. Dumot, J. Ponsky, G. Gelikonov, B. Davros, E. Donchenko, and J. Richter, "Optical coherence tomography of the esophagus and proximal stomach in health and disease," *Am. J. Gastroenterol.* **96**(9), 2633–2639 (2001).
  40. J. M. Schmitt, S. L. Lee, and K. M. Yung, "An optical coherence microscope with enhanced resolving power in thick tissue," *Opt. Commun.* **142**, 203–207 (1997).